Journal of Mines, Metals and Fuels, *71(12C) : 49-57; 2023. DOI: 10.18311/jmmf/2023/47260*

Print ISSN : 0022-2755

Journal of Mines, Metals and Fuels

Contents available at: *www.informaticsjournals.com/index.php/jmmf*

Numerical Investigation on Forchheimer MHD Non-Newtonian Fluid over an Exponential Stretching Sheet with Joule and Viscous Dissipation

P. A. Dinesh[1*], R. Sumithra[2], K. R. Roopa[1], Sweeti Yadav[1], K. Ashok Kumar[3], M. A. Archana[2], M. Hanumantha[2], H. R. Chandrashekar[2], H. S. Charan[2] and M. Mohammed Suhail[2]

[1]Department of Mathematics, M S Ramaiah Institute of Technology, Bengaluru – 560054, Karnataka, India; dineshdpa@msrit.edu, krroopa870@gmail.com, sweetiyadav1989@gmail.com

[2]Department of Mathematics, Nrupathunga University, Bengaluru – 560001, Karnataka, India; sumitradiya@yahoo.com, archanamurthy78@gmail.com, hanumantham57@gmail.com, chandrashekarhr1234@gmail.com, mdsuhail302000@gmail.com

[3]Department of Mechanical Engineering, M S Ramaiah Institute of Technology, Bengaluru – 560054, Karnataka, India; ashok@msrit.edu

Abstract

We investigate the synergistic consequences of Ohmic heating and viscous degradation on unsteady MHD flow across an extensible sheet immersed in fluid with pores. For the various assumptions on the real problem, a physical model led us to a non-linear coupled partial differential equation which is then transformed to ordinary differential equation using similarity technique. The computational work is carried out using shooting technique compresses of Runge-Kutta-Felhberg method with Newton-Raphson iterative scheme to solve the non-linear coupled ordinary differential equations with converting a boundary value problem to initial value problem by choosing a guess value. A study is conducted on governing parameters, including the Biot number, Weissenberg number, Eckert number, Joule consequences, unsteadiness, and Forchheimer number. Graphics are used to show how these characteristics affect concentration, velocity, and temperature.

Keywords: *Exponential Stretching Sheet, Non-Newtonian Fluids, Forcheimmer Term, MHD, Viscous and Joule Dissipation*

1.0 Introduction

Numerous studies have revealed that flow across a stretched sheet is driven by a linear change in the stretching rate of the sheet. As a result, despite the fact that this flow occurs often in many technological applications, the limit layer flow Consequences by an exponentially stretched sheet has received little attention. Flow of a MHD boundary layer over an exponentially stretching sheet in the presence of radiation has been investigated by Salah and Almohammadi[1]. Seini and Makinde[2] studied the consequences of a chemical reaction due to an exponential stretching surface caused by radiation on MHD boundary layer flow. The increased values of the transverse magnetic field and radiation parameters have been shown to decrease the surface heat transfer rate. Mukhopadhyay[3] presents computational methods for transferring heat and constant MHD flow through the boundary layer using an exponentially stretched surface immersed in a thermo layered medium under suction.

**Author for correspondence*

He also examined the Consequences of partial slip rather than absence of slip on MHD flow through the boundary layer through a permeable exponentially extending surface employing suction or injection. The peculiar characteristics of nanomaterials are caused by the existence of zinc (Zn), copper (Cu), manganese (Mn), iron (Fe), titanium dioxide (Ti) and other metallic nanoparticles. Bhattacharyya and Layek[4] examined the nanofluid flow pattern in the boundary zone caused by an exponentially reducing sheet. Eid[5] examined the behavior of a nanofluid's mixed conduction flow from the boundary layer across a medium with pores caused by an exponentially extending sheet when a magnetic field was applied, a chemical reaction was occurring, and heat was being generated or absorbed. Recently, many authors[6-10] have contributed to the studies concerning flow phenomena past exponential stretching sheet.

The significance of other than Newtonian fluid flows in engineering as well as commerce has attracted a lot of attention in recent decades. Non-Newtonian liquids with mass and heat transfer are significantly used in the preparation of food, manufacturing paper, and lubricating operations. The scientific community has created a wide range of non-Newtonian models as a result of the extensive application of unconventional fluids in business. Casson and Carreau fluids are non-Newt0nian fluids. Raju and Sandeep[11] suggested a theoretical framework to examine how nonlinear heating radiation affects the multidimensional flow of Casson and Carreau liquids through an elastic surface in the presence of irregular heat sources and sinks and homogeneous-heterogeneous reactions. Gireesha *et al.*[12] examined the multidimensional hydromagnetic convective flow of Casson-Carreau liquids with homogeneous–heterogeneous actions, viscous dissipation, irregular radiation, and joule heating. Sobamowo *et al.*[13] investigated the joint Consequences of influenced by temperature, internal warmth generation, slanted magnetic field, and heating radiation on irregular two-dimensional circulation and heat transfer study of dissipative Casson-Carreau nano liquid on a stretched sheet enmeshed in a material with pores. Nagendra *et al.*[14] Studied the two-dimensional magneto-hydrodynamic Casson and Carreau fluid flowing past a circular cylinder under the slip consequences.

Many applications, such as fermentation, grain storage, groundwater contamination, reservoir movement, petroleum production, groundwater sources, fossil fuel systems, nuclear waste disposal, energy storage units, oil resources, solar panels, and many more, benefit greatly from the flow of porous medium. Many research pertaining to porous medium with low porosity and fluid velocities were based on Darcy's hypothesis; however, it was not applicable to media with high permeability and bigger transit. The classical Darcy's law does not take into consideration inertial and edge conditions at high flow speeds. For this reason, Darcy's hypothesis was unable to explain the physical conditions involving high porosity medium and velocities. Forchheimer addressed this flaw by adding a square velocity component to the Darcy velocity model, which made it possible to calculate inertia and boundary properties. Hayat *et al.*[15] have dealt with the issue of thermophoresis and Darcy-Forchheimer circulation of a viscoelastic nanofluid technology in an exponentially extending concave sheet with Brownian motion. Das *et al.*[16] studied the Consequencess of heat source/sink, joule heating and viscous dissipation in the Darcy–Forchheimer flow of a magneto-couple stress fluid over an inclined exponentially stretching sheet. In addition the outermost layer of a tilted exponentially expanding sheet inserted into a medium that is porous, a combined investigation of the Consequences of the magnetic field that is produced as well as chemical interactions with the Darcy-Forchheimer connection on the transfer of heat and mass in unconventional third-grade fluid is discussed numerically by Abbas *et al.*[17]. Sharma[18] investigated the Consequences of Darcy-Forchheimer MHD flow of blood-based nanofluids in an exponentially stretched sheet. Senapati *et al.*[19] examined the effects of homogenous heat source, ohmic effect, solar radiation, and viscosity dissipation on the MHD motion of a Casson fluid through an irregularly permeable stretched sheet encased in a material that is permeable. Alqahtani *et al.*[20] examined the Casson nanofluid hybrid flow through a wider stretched sheet exposed to an inclined magnetic field, taking into account temperature and velocity slip circumstances, heat absorption, viscosity dissolution, heat transfer, the Darcy-Forchheimer Consequences, and thermophoresis diffusion.

Investigating the synergistic Consequences of Ohmic heating and viscous degradation on unstable flow through an exponential stretching sheet with Casson and Carreau fluids in a porous medium with Darcy-Forchheimer correlation is the goal of the current work.

2.0 Mathematical Formulation

Assume a continuous, incompressible, two-dimensional flow of Carreau and Casson streams in the direction of an exponential expanding surface. The y-axis, on the other hand, is perpendicular to the outer layer and the x-axis is passed via an elastic sheet in the plane of flow. In the x-axis, the exponential sheet of expansion is assumed with velocity $U_W = Ue^{\frac{Nx}{L}}$ elucidate at $y = 0$, where exponential parameter is N and length is L. The current concept is thought to address the Casson flow and Carreau flow when $n = 1$ and when $\beta \to \infty$ respectively. Brownian motion phenomena and thermophoresis are also taken into account. As seen in Figure 1, B_0 is taken in y direction.

The following outline of the equations that govern the boundary layer is based on the aforementioned assumptions:

$$\frac{\partial u}{\partial x} + \frac{\partial v}{\partial y} = 0 \quad (1)$$

$$U\frac{\partial u}{\partial x} + V\frac{\partial u}{\partial y} = \nu\left(1 - \frac{1}{\beta}\right)\frac{\partial^2 u}{\partial y^2} + \frac{3\nu(n-1)\Gamma^2}{2}\left(\frac{\partial u}{\partial y}\right)^2\frac{\partial^2 u}{\partial y^2} - \frac{\sigma B_x^2}{\rho_f}u - \frac{\nu}{k^*}u - Fu^2 \quad (2)$$

$$\frac{\partial T}{\partial x} + v\frac{\partial T}{\partial y} = \alpha\frac{\partial^2 T}{\partial y^2} + \tau\left[D_B\frac{\partial c}{\partial y}\frac{\partial T}{\partial y} + \frac{D_T}{T_\infty}\left(\frac{\partial T}{\partial y}\right)^2\right] + \frac{\mu}{\rho C_p}\left(\frac{\partial u}{\partial y}\right)^2 + \frac{Q_0}{\rho C_p}(T - T_\infty) - \frac{\sigma B_0^2 U^2}{\rho_0 C_p} \quad (3)$$

$$\frac{\partial c}{\partial x} + v\frac{\partial c}{\partial y} = D_B\frac{\partial^2 c}{\partial y^2} + \left(\frac{D_B}{T_\infty}\right) + \frac{\partial^2 T}{\partial y^2} + \gamma(c - c_\infty)^n \quad (4)$$

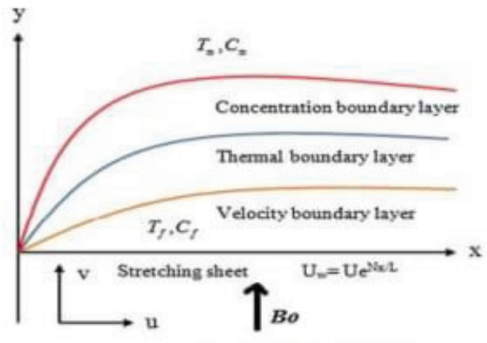


Figure 1. Physical model.

Here *u, v* represents the velocity components in the *x, y* directions respectively P_f- fluid flow density, *V*-kinematic viscosity, $k^* = k_0 e^{-\frac{Nx}{L}}$ represent the permeability, k_0 is constant which gives initial permeability, σ -electric conductivity, τ - material constant, $(\rho C)_f$ - heat capacity, *c*- fluids concentration, $(\rho C)_p$ - heat capacity with fixed pressure, $\tau = \frac{(\rho C)_p}{(\rho C)_f}$, $\alpha = \frac{\kappa}{\rho C_f}$ - thermal diffusivity, *T*- Temperature, T_∞- ambient temperature, D_∞- Brownian diffusion, β- Casson parameter, and D_T - thermophoresis diffusion. $B(x) = B_0 e^{\frac{Nx}{2L}}$, applied magnetic field where B_0 being constant.

Subjected boundary conditions are:

$$\left.\begin{aligned} &u = U,\ v = 0,\ -\kappa\frac{\partial T}{\partial y} = h_f(T_f - T) \\ &D_B\frac{\partial c}{\partial y} + \frac{D_T}{T_\infty}\frac{\partial T}{\partial y} = 0 \ \text{ at } \ y = 0 \\ &u \to 0,\ v \to 0,\ T = T_\infty,\ c = c_\infty \ \text{ as } \ y \to \infty \end{aligned}\right\} \quad (5)$$

The classification of the similarity transformations is:

$$\left.\begin{aligned} &u = U_W = Ue^{\frac{Nx}{L}}f'(\eta),\ \eta = y\sqrt{\frac{U}{2\nu L}}e^{\frac{Nx}{L}}, \\ &\mathrm{v} = -\sqrt{\frac{\nu U}{2L}}e^{\frac{Nx}{2L}}\{f(\eta) + \eta f'(\eta)\} \end{aligned}\right\} \quad (6)$$

Equation (1), which is automatically fulfilled, using (6), (2-4) then converted to

$$\left(1 + \frac{1}{\beta}\right)f''' + N\left[ff'' - 2(f')^2\right] + \frac{3(n-1)}{2}We\,f'''(f'')^2 - Mf' = 0 \quad (7)$$

$$\theta'' + \frac{N\,\mathrm{Pr}}{1+R}(f'\theta' - \theta' f) + \frac{Nb}{1+R}\theta'\phi' + \frac{Nt(\theta')^2}{1+R} + \frac{\mathrm{Pr}\,Ec}{1+R}\frac{(f'')^2}{(f')^2} - \frac{M\,\mathrm{Pr}\,Ec}{1+R} + \frac{\mathrm{Pr}\,\alpha\,\theta 2\nu L f'}{U_W(1+R)} = 0 \quad (8)$$

$$\theta'' + Sc\,N\left[f'\theta' - \theta' f\right] + \frac{Nt}{Nb}\phi'' + \frac{Sc\,\gamma\left(c-c_\infty\right)^{n-1} f'(\phi)^n}{U_W} = 0 \tag{9}$$

With boundary conditions being

$$\left.\begin{aligned} &f(0)=0,\ f'(0)=0,\ \theta'(0) \\ &=-Bi\left(1-\theta(0)\right),\ Nb\phi'(0)+Nt\theta'(0)=0 \end{aligned}\right\} \tag{10}$$

$$f'(\eta)\to 0,\ \theta'(\eta)\to 0 \ \text{ as } \ \eta\to\infty \tag{11}$$

where , Prandtl Number $\Pr = \frac{\nu}{\alpha}$, Magnetic Parameter $M = \frac{2\sigma B_0^2 L}{U\rho} = \frac{(\rho C)_p}{(\rho C)_f}$,

$Nb = \frac{D_B\left(c_f - c_\infty\right)(\rho C)_p}{\nu(\rho C)_f}$ is the Brownian motion Parameter, $Nt = \frac{D_T\left(T_f - T_\infty\right)}{T_\infty \nu(\rho C)_f}$ is the thermophoresis parameter, $We = \frac{U^3 e^{3x/L}\Gamma^2}{\nu L}$ is the Weisenberg number, $Sc = \frac{\nu}{D_B}$ is the Schmidt number. Nusselt number and drag coefficient are as follows:

$c_f = \frac{\tau_W}{\rho U_W^2}$ where

$$\tau_w = \left(1+\frac{1}{\beta}\right)\left(\frac{\partial u}{\partial x}\right) + \frac{(n-1)\Gamma^2}{2}\left(\frac{\partial u}{\partial y}\right)^3,$$

$$Nu_x = \frac{x q_w}{\kappa\left(T_f - T_\infty\right)} \tag{12}$$

where $q_w = -\kappa\left(\frac{\partial T}{\partial u}\right)_{y=0}$ (13)

From equations (12) and (13), by using equation (6) we get

$$\sqrt{\mathrm{Re}}\,c_f = \left(1+\frac{1}{\beta}\right)f'(0) + \frac{(n-1)We^2}{2}\left(f'(0)\right)^3,\ \sqrt{\frac{2}{\mathrm{Re}}}\,Nu_x = -\theta'(0) \tag{14}$$

where local Reynolds number, $\mathrm{Re} = \frac{U_W L}{\nu}$.

3.0 Solution Procedure

The shooting technique is a numerical method used to solve Ordinary Differential Equations (ODEs) or boundary value problems by transforming them into initial value problems. It involves "shooting" an initial guess for the unknown variables and adjusting it iteratively until the desired boundary conditions are satisfied. Here's a basic overview of how the shooting technique works. If you have a boundary value problem, transform it into an initial value problem by guessing one boundary condition and treating the other as an unknown parameter. Make an initial guess for the unknown parameter(s) and solve the resulting initial value problem using a numerical ODE solver (e.g., Runge-Kutta methods) to obtain a solution. Compare the solution obtained from the initial value problem with the desired boundary condition that you didn't use for the initial guess. Once the answer has been achieved fits the required boundary condition within a given tolerance, adjust the estimated parameter and continue steps repeatedly. You have discovered a numerical solution to the initial boundary value problem after the solution converges to the required boundary condition. The success of the shooting technique depends on the initial guess and the behavior of the solution. It's a trial-and-error process that requires careful adjustments and convergence monitoring.

4.0 Graphs and Discussion

The influence for various non-dimensional parameters involved in the study of the fluid flow, temperature is illustrated with graphs. For the distinct values, the numerical findings of the Schmidt number (*Sc*), Forchheimer number (*F*), Weissenberg number (*We*), and magnetic parameter (*M*) are also reported. The non-linear ordinary differential equation is solved in terms of boundary conditions. (Numerically) [Using dimensionless parameters such as the magnetic parameter (M), Sc, and We].

The fluctuations in Biot number on the thermal field and mass diffusion fields are illustrated in Figures 2 and 3. We are aware that the mass diffusion fields and temperature have a direct relationship with the Biot number. Thus, it is evident that rising Biot numbers also result in rising mass diffusion and temperature values. Temperature differences generally grow with increasing levels of the Biot number.

Figure 4 The graph shows how the dimensionless parameter θ(η), with respect to *E*, varies with the dimensionless parameter η, which represents the ratio of the characteristic time to the relaxation time. How long does a fluid take to react to an alteration in its shear rate is measured by its characteristic time, and the relaxation time is a measure of how long it takes for the fluid to return to its original state after being sheared. The graph compares the curves for Casson fluid (solid red) and Carreau fluid (dashed black) for different values of n, which is the power index that controls how fast the viscosity changes with shear rate. The graph shows that for both models, θ(η) decreases as η increases. However, the rate of decrease is different for each model and each value of n. For Casson fluid, θ(η) drops sharply from 1 to 0 as η increases from 0 to 1, meaning that there is a sudden change in viscosity at a critical shear rate. For Carreau fluid, θ(η) decreases gradually from 1 to 0 as η increases from 0 to infinity, meaning that there is a smooth transition in viscosity over a wide range of shear rates. The value of n affects how steep or flat the curve is: for higher values of n, θ(η) decreases more slowly, meaning that the viscosity is more sensitive to shear rate; for lower values of n, θ(η) decreases more quickly, meaning that the viscosity is less sensitive to shear rate. The inset graph in the top right corner shows how θ(η) varies with η for different values of E, which is another dimensionless parameter that represents the ratio of the yield stress to the characteristic stress. The characteristic stress is a measure of how much force is needed to deform the fluid by a certain amount. The inset graph only applies

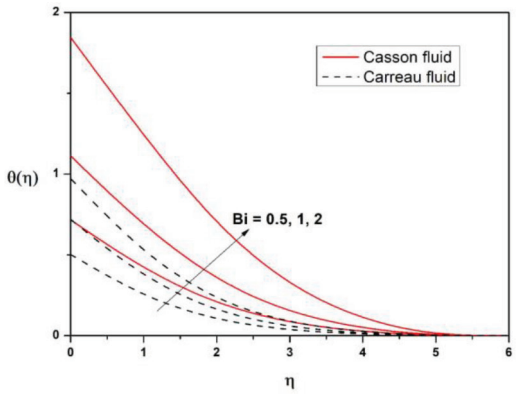


Figure 2. Consequences of Bi upon temperature.

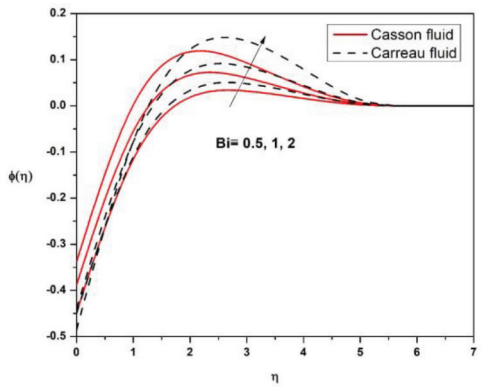


Figure 3. Consequences of Bi upon concentration.

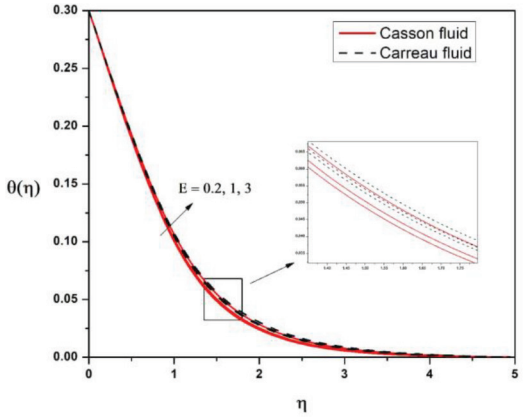


Figure 4. Consequences of E upon temperature.

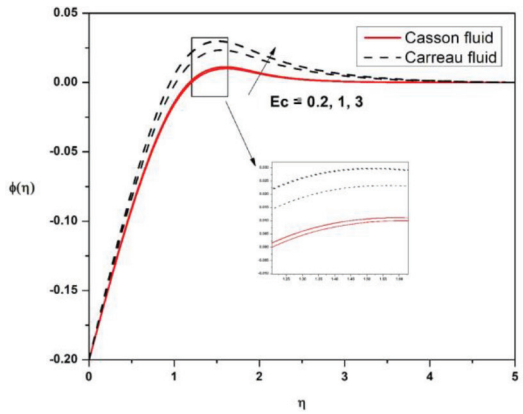


Figure 5. Consequences of Ec upon concentration.

to Casson fluid, since Carreau fluid does not have a yield stress. The graph shows that for higher values of E, θ(η) drops more sharply, meaning that the yield stress is higher and the fluid behaves more like a solid at low shear rates; for lower values of E, θ(η) drops more gently, meaning that the yield stress is lower and the fluid behaves more like a liquid at low shear rates.

Figure 5 shows how the dimensionless function φ(η) varies with the dimensionless parameter η for both fluids. The parameter η represents the ratio of the characteristic time to the relaxation time. The characteristic time is a measure of how long it takes for a fluid to respond to a change in shear rate, and the relaxation time is a measure of how long it takes for a fluid to return to its original state after being deformed. The graph shows that for both fluids, φ(η) decreases as φ(η) increases, which means that both fluids have a shear-thinning behavior. However, the graph also shows that Casson fluid has a higher peak value φ(η) than Carreau fluid, which means that Casson fluid has a higher yield stress and requires more force to start flowing. The graph also shows that Carreau fluid has a lower asymptotic value of φ(η) than Casson fluid, which means that Carreau fluid has a lower viscosity at high shear rates and flows more easily. The inset graph shows how φ(η) varies with η for different values of Ec, which is the Eckert number. The Eckert number is a dimensionless number that represents the ratio of kinetic energy to enthalpy difference. It measures the Consequences of heat generation due to viscous dissipation. The inset graph shows that for Casson and Carreau fluids, φ(η) increases as Ec increases, which means that heat generation increases the apparent viscosity and makes the fluid more resistant to flow.

Figure 6 shows two curves, one solid red and one dashed black. The x-axis is labeled "η" and the y-axis is labelled "f(η)". The red curve is labelled "Casson fluid" and the black curve is labelled "Carreau fluid". The red curve starts at (0,1) and decreases to (5,0.4). The black curve starts at (0,0.8) and decreases to (5,0.2). There is a small inset graph in the top right corner of the main graph. This inset graph shows a zoomed in view of the curves between η = 1.85 and η = 2.0. The inset graph has the same x and y axis labels as the main graph. The inset graph shows the red curve crossing over the black curve at around η = 1.9.

Figure 7 is a plot of two curves, one solid red and one dashed black, plotted against a white background. The x-axis is labeled "η" and the y-axis is labeled "θ(η)". The red curve is labeled "Casson fluid" and the black curve is labeled "Carreau fluid". The curves intersect at two points, one near the origin and one near the top right corner of the graph. The graph has a small inset graph in the top right corner, which shows a magnified view of the curves near the origin. The inset graph has the same axis labels as the main graph. The graph has a label "F = 0.5, 0.7, 1" near the bottom left corner.

Figure 8 shows how the concentration term ϕ(n) varies with the Forchheimer term F for both Casson and Carreau fluids. The solid line indicates the Casson fluid and the dashed line indicates the Carreau fluid. The curves intersect at three points, which indicate the values of F and ϕ(n) where the two fluids have the same viscosity. These points are labeled F = 0.5, 0.7, 1. The inset graph in the lower right corner shows a magnified view of the intersection points.

Figure 9 illustrates some of the differences between Casson and Carreau fluids. For example, Casson fluid has a higher viscosity than Carreau fluid at

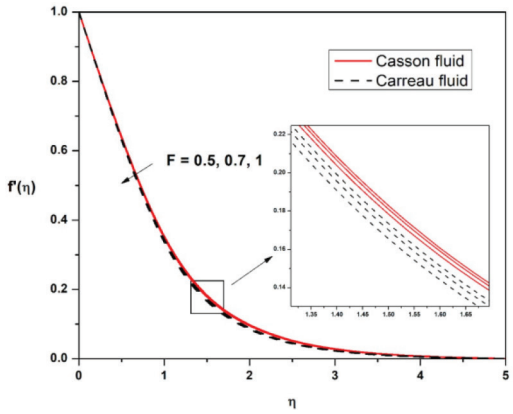


Figure 6. Consequences of F upon velocity.

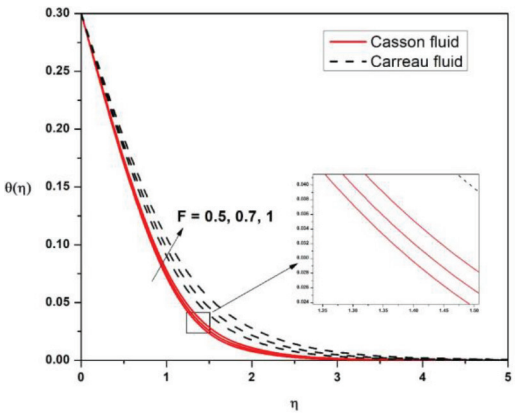


Figure 7. Consequences of F upon temperature.

low Forchheimer terms, but a lower viscosity at high Forchheimer terms. Carreau fluid has a more gradual change in viscosity than Casson fluid, which has a sharp drop after the yield stress. The graph also shows that there are some values of F where the two fluids have the same viscosity, which may be useful for some applications.

The thermal field and mass diffusion fields are shown to vary for various magnetic field strengths in Figures 9 and 10. It results in opposite to that of velocity field i.e., temperature and concentration field grows with enhancing values of *M*.

The velocity vectors when the magnetic field parameters change are displayed in Figure 11. It is observed that the field of velocity reduces as the value increases. Typically, an increase in the field of magnetism produces a force of resistance that opposes the flow. Lorentz force is the name for the power that resists the flow of energy.

Figures 12 and 13 are respectively the plots of temperature and mass diffusion fields against η for different Weissenberg number (*We*). Here we know that Wessinberg number is directly proportional to the time constant and it is larger for raising the values of *We*, as a result temperature and mass diffusion fields are declined. As η increases, $\theta(\eta)$ gradually decreases to zero, whereas reverse Consequences is observed in case of $\phi(\eta)$.

Figure 14 shows that both Casson and Carreau fluids have higher shear stress than Newtonian fluids at low shear rates, but lower shear stress than Newtonian fluids at high shear rates. The red line indicates the Casson fluid model, and the black line indicates the Carreau fluid model. The arrows on the graph indicate different values of J, which is a dimensionless parameter that represents the ratio of viscous forces to elastic forces in the fluid.

Figure 15 shows the relationship between a dimensionless parameter η and a function φ(η) for

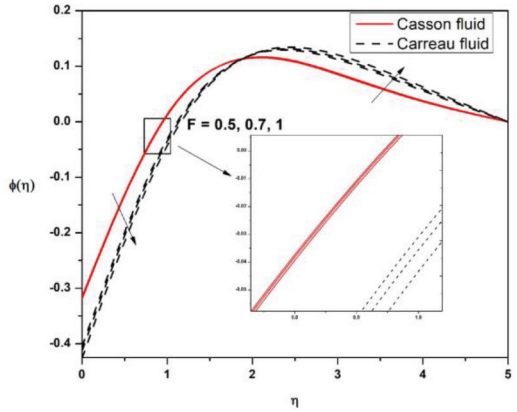


Figure 8. Consequencess of F upon concentration.

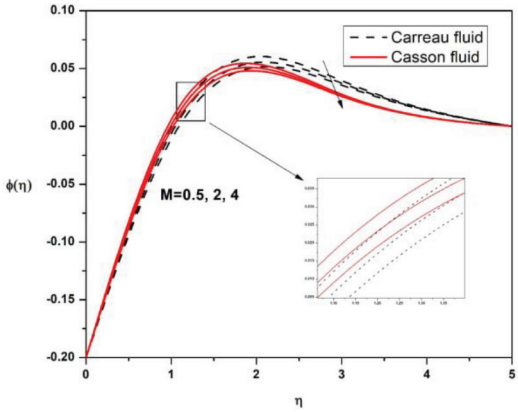


Figure 10. Consequences of M upon concentration.

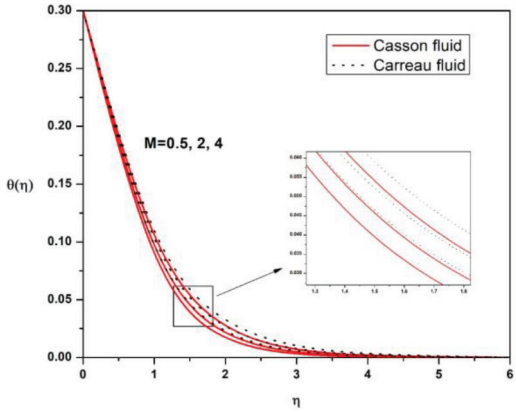


Figure 9. Consequences of M upon temperature.

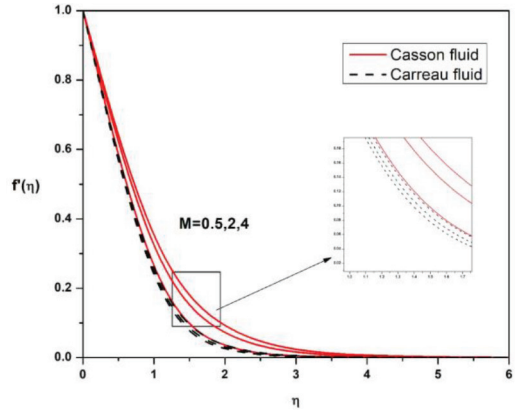


Figure 11. Consequences of M upon velocity.

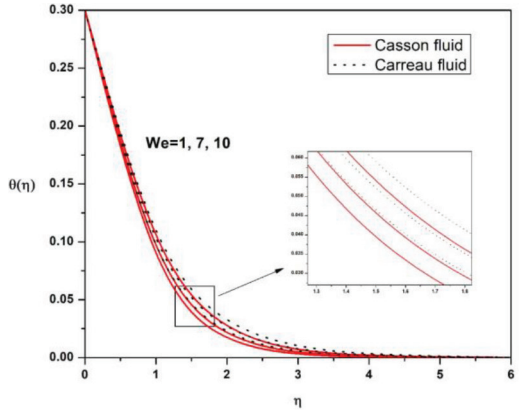


Figure 12. Consequences of We upon temperature.

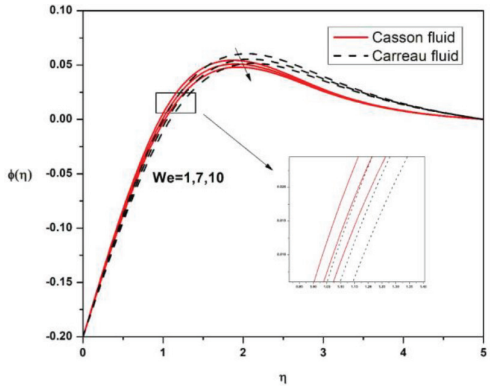


Figure 13. Consequences of We upon concentration.

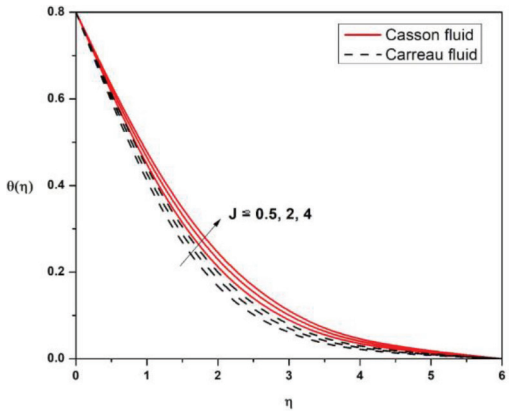


Figure 14. Consequences of J upon temperature.

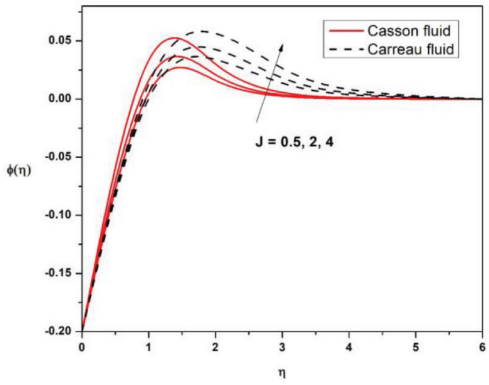


Figure 15. Consequences of J upon concentration.

both Casson fluid and Carreau fluid. The parameter η is related to the ratio of the boundary shear stress to the capitulate stress for Casson fluid, and to the ratio of the wall shear rate to the relaxation time for Carreau fluid. The function φ(η) is related to the velocity profile of the fluid in a pipe. The graph has two vertical lines at J = 0.5 and J = 2.4, which correspond to two different values of another dimensionless parameter J. This parameter J is related to the ratio of the pressure gradient to the yield stress for Casson fluid, and to the ratio of the pressure gradient to the zero-shear viscosity for Carreau fluid. The graph shows that for both Casson fluid and Carreau fluid, φ(η) increases as η increases, but at different rates. The red curve (Casson fluid) is smoother than the black curve (Carreau fluid), which has some jagged parts. The curves intersect at two points, one near the origin and one near the top right corner of the graph. The intersection points indicate that there are some values of η for which both fluids have the same value of φ(η).

5.0 Conclusions

We investigate the synergistic Consequences of Ohmic heating and viscous degradation on unsteady MHD flow across an extensible sheet immersed in fluid with pores, magnetic fields, Forchheimer. The governing equations are solved using shooting procedure with fourth-order Runge-Kutta methods - Numerically The important points are as follows:

- The mass transfer gradient increases as the Schmidt number (Sc) and magnetic parameter (M) increase.
- When compared to casson fluid, the Lorentz force has a strong influence on Carreau fluid.
- Positive values of the temperature and space dependent forchheimer parameter act as heat generators.

6.0 References

1. Salah F, Almohammadi A. MHD boundary layer flow due to an exponentially stretching surface through porous

medium with radiation effect. Int J Adv Appl Sci. 2023; 10(11):165-70. https://doi.org/10.21833/ijaas.2023.11.020
2. Seini YI, Makinde OD. MHD boundary layer flow due to exponential stretching surface with radiation and chemical reaction. Math Probl Eng. 2013; 2013:1-7. https://doi.org/10.1155/2013/163614
3. Mukhopadhyay S. Slip effects on MHD boundary layer flow over an exponentially stretching sheet with suction/blowing and thermal radiation. Ain Shams Eng J. 2013; 4(3):485-91. https://doi.org/10.1016/j.asej.2012.10.007
4. Bhattacharyya K, Layek GC. Magnetohydrodynamic boundary layer flow of nanofluid over an exponentially stretching permeable sheet. Phys Res Int. 2014; 2014:1-12. https://doi.org/10.1155/2014/592536
5. Eid MR. Chemical reaction effect on MHD boundary-layer flow of two-phase nanofluid model over an exponentially stretching sheet with a heat generation. J Mol Liq. 2016; 220:718-25. https://doi.org/10.1016/j.molliq.2016.05.005
6. Yahaya RI, Md Arifin N, Mohamed Isa SSP, Rashidi MM. Magnetohydrodynamics boundary layer flow of micropolar fluid over an exponentially shrinking sheet with thermal radiation: Triple solutions and stability analysis. Math Methods Appl Sci. 2021; 44(13):10578-608. https://doi.org/10.1002/mma.7432
7. Arshad M, Hussain A, Hassan A, Haider Q, Ibrahim AH, Alqurashi MS, *et al*. Thermophoresis and brownian effect for chemically reacting magneto-hydrodynamic nanofluid flow across an exponentially stretching sheet. Energies. 2021; 15(1):143. https://doi.org/10.3390/en15010143
8. Goud BS, Reddy YD, Mishra S. Joule heating and thermal radiation impact on MHD boundary layer Nanofluid flow along an exponentially stretching surface with thermal stratified medium. Proc Inst Mech Eng Part N J Nanomater Nanoeng Nanosyst. 2023; 237(3-4):107-19. https://doi.org/10.1177/23977914221100961
9. Mansoor M, Nawaz Y, Ul-Hassan Q. Non-similarity method for heat and mass transfer of MHD radiative flow over exponentially stretching sheet. Therm Sci. 2022; 26(5 Part A):3703-14. https://doi.org/10.2298/TSCI210505309M
10. Amjad M, Khan MN, Ahmed K, Ahmed I, Akbar T, Eldin SM. Magnetohydrodynamics tangent hyperbolic nanofluid flow over an exponentially stretching sheet: Numerical investigation. Case Stud Therm Eng. 2023; 45:102900. https://doi.org/10.1016/j.csite.2023.102900
11. Raju CSK, Sandeep N. Unsteady three-dimensional flow of Casson-Carreau fluids past a stretching surface. Alexandria Eng J. 2016; 55(2):1115-26. https://doi.org/10.1016/j.aej.2016.03.023
12. Gireesha BJ, Kumar PBS, Mahanthesh B, Shehzad SA, Rauf A. Nonlinear 3D flow of Casson-Carreau fluids with homogeneous-heterogeneous reactions: A comparative study. Results Phys. 2017; 7:2762-70. https://doi.org/10.1016/j.rinp.2017.07.060
13. Sobamowo G, Adesina OA, Jayesimi L. Magnetohydrodynamic flow of dissipative Casson-Carreau nanofluid over a stretching sheet embedded in a porous medium under the influence of thermal radiation and variable internal heat generation. Eng Appl Sci Lett. 2019; 2(2):18-36. https://doi.org/10.30538/psrp-easl2019.0018
14. Nagendra N, Venkateswarlu B, Boulahia Z, Amanulla CH, Ramesh GK. Magneto Casson-Carreau fluid flow through a circular porous cylinder with partial slip. J Appl Comput Mech. 2022; 8(4):1208-21.
15. Hayat T, Haider F, Muhammad T, Alsaedi A. Numerical study for Darcy-Forchheimer flow of nanofluid due to an exponentially stretching curved surface. Results Phys. 2018; 8:764-71. https://doi.org/10.1016/j.rinp.2018.01.010
16. Das S, Ali A, Jana RN. Darcy-Forchheimer flow of a magneto-radiated couple stress fluid over an inclined exponentially stretching surface with Ohmic dissipation. World J Eng. 2021; 18(2):345-60. https://doi.org/10.1108/WJE-07-2020-0258
17. Abbas A, Shafqat R, Jeelani MB, Alharthi NH. Significance of chemical reaction and Lorentz force on third-grade fluid flow and heat transfer with Darcy-Forchheimer law over an inclined exponentially stretching sheet embedded in a porous medium. Symmetry (Basel). 2022; 14(4):779. https://doi.org/10.3390/sym14040779
18. Sharma S. MHD boundary layer flow past an exponentially stretching sheet with Darcy-Forchheimer flow of nanofluids. Indian J Sci Technol. 2022; 15(33):1594-604. https://doi.org/10.17485/IJST/v15i33.607
19. Senapati M, Parida SK, Swain K, Ibrahim SM. Analysis of variable magnetic field on chemically dissipative MHD boundary layer flow of Casson fluid over a nonlinearly stretching sheet with slip conditions. Int J Ambient Energy. 2022; 43(1):3712-26. https://doi.org/10.1080/01430750.2020.1831601
20. Alqahtani AM, Bilal M, Usman M, Alsenani TR, Ali A, Mahmuod SR. Heat and mass transfer through MHD Darcy Forchheimer Casson hybrid nanofluid flow across an exponential stretching sheet. Zeitschrift für Angew Math und Mech. 2023; 103(6). https://doi.org/10.1002/zamm.202200213